Optics & Laser Technology 171 (2024) 110435

Contents lists available at ScienceDirect

Optics and Laser Technology

journal homepage: www.elsevier.com/locate/optlastec

Full length article

Influence of mineral composition on thermal equilibrium state during laser perforation

Xiaofeng Yang [a,b,*], Aiguo Nie [b], Fatao Si [b], Derek Elsworth [c], Jiaheng Zhou [b]

[a] School of Aerospace Engineering, Beijing Institute of Technology, Beijing 100081, China
[b] School of Mechanics and Civil Engineering, China University of Mining and Technology, Beijing 100083, China
[c] Department of Energy and Mineral Engineering, EMS Energy Institute and G3 Center, Pennsylvania State University, University Park, PA, USA

ARTICLE INFO

Keywords:
Laser rock perforation
Melt properties
Mineral compositions
Equilibrium stage

ABSTRACT

Energy consumption during laser rock perforation is controlled by conductive losses and latent heats during the phase transitions of melting and evaporation. To understand then improve the efficiency of laser perforation, the influence of rock mineral composition on these processes is investigated, and a theoretical model of laser rock breaking under steady-state heat conduction is developed. The findings reveal that the melting properties of mineral components primarily control thermal equilibrium during laser perforation. The key minerals, namely feldspar, quartz, and clay, were used to study the melt response in both pure samples and synthetic rock composites composed of these minerals. When feldspar is dominant, the thermal equilibrium temperature remains stable after reaching the feldspar gas phase boundary. While in situations where quartz dominates, the thermal equilibrium temperature is slightly below the melting point of pure quartz. The findings highlight the relationship between laser rock perforation efficiency and melting properties of minerals.

1. Introduction

Laser-induced breaking of rock is much anticipated because of its high efficiency in perforating, especially when applied to hard/brittle rocks [1,2]. Application of the laser weakens the rock through the creation of defects, which reduce the resistance to macroscale breakage [3]. Laser-induced rock breaking is advantageous when it can result in energy savings, enhance resource exploitation efficiency, and contribute to sustainable resource development. However, a significant amount of energy is frequently dissipated in the phase transformation of certain rock constituents, rather than contributing to the brittle fracture of rock. This substantially elevates the overall energy consumption of the process. The role of various rock properties in modulating this energy absorption and consumption response remains unclear, and are addressed in this investigation.

In laser rock perforation, electromagnetic energy is focused and absorbed on the exposed surface, where it is converted into thermal energy extending to a specific depth beneath the rock surface [4]. At low energy levels, this localized heat is conducted into the interior and results in a temperature gradient [5,6]. The resulting thermal stresses promote failure as a result of brittle thermal spallation [7–11]. At higher energy levels, or for longer exposure, the constituent minerals will reach their phase transition temperature and begin to both melt and then evaporation, resulting in plastic failure [12–15]. Irrespective of the specific mechanism, whether it's brittle or plastic, failure is governed by the laser's parameters and the reactions of both individual and aggregate mineral constituents within the rock.

Rock properties predominantly influence the achieved temperature, as well as the depth and efficiency of laser perforation. High thermal conductivity in the rock leads to rapid heat conduction, thereby lowering the specific energy (SE) needed for rock breaking [16]. When the rock comprises smaller pores and defects, a higher thermal expansion coefficient, or a lower fracture toughness, renders it more susceptible to brittle rupture [17–19]. Rock type also affects the form of rock failure and the products of the laser irradiation. Limestone is mainly composed of calcium carbonate, which will decompose and evaporate rather than melt during laser perforation [20–22]. Conversely, basalt will melt to form a glazed layer [23]. Granite and sandstone will produce observable evaporation at the rock-laser interface when the rock reaches critical temperature [24]. Thus, the resulting rock temperature is a critical factor that controls the products of laser rock breakage and in turn is controlled by the intensity and duration of the irradiation. Although these trends are evident, little confirmatory evidence is available on the systematic influence of rock composition and resulting

* Corresponding author at: School of Aerospace Engineering, Beijing Institute of Technology, Beijing 100081, China.
E-mail address: xfyang@bit.edu.cn (X. Yang).

https://doi.org/10.1016/j.optlastec.2023.110435
Received 21 June 2023; Received in revised form 4 November 2023; Accepted 8 December 2023
Available online 13 December 2023
0030-3992/

rock temperature on the efficiency of laser perforating.

This deficit is addressed here through laser perforation experiments on rocks and artificial rock samples. These experiments aimed to investigate the influence of the thermophysical properties of different minerals and melt properties on laser rock perforation. The process of thermal equilibration during laser perforation and its effect on SE are described. Furthermore, the observations from these experiments were systematically organized and analyzed using a heat transfer model to offer a comprehensive assessment of the underlying mechanisms.

2. Experimental materials and procedures

The continuous wave CO_2 laser perforator was adopted for the experiments with an irradiation radius of 2 mm at a distance of 160 mm (Fig. 1). The maximum power of the laser was 50 W. K-type, B-type, and platinum–rhodium thermocouples are simultaneously adopted to measure rock temperature from 0℃ to 2200℃. The measurement point was 3 mm away from the sample center, and the sampling frequency was 1200 Hz.

Laser perforation experiments were performed on individual samples of granite, sandstone and basalt. The cylindrical rock samples are 50 mm in diameter and 25 mm in height and underwent mineral composition analysis by X-ray diffraction (XRD) techniques (Table 1). The principal clay minerals present in all three rock samples are illite and kaolinite.

In addition, we conducted experiments on synthetic aggregates designed to emulate the three rock types. In these aggregates, quartz, feldspar, and kaolinite were deliberately chosen as representative mineral components to mirror the primary constituents of granite, basalt, and sandstone. The melting and evaporation temperatures of the three components are reported in Table 2.

Artificial rock samples with different mineral compositions were fabricated using high-temperature-resistant inorganic adhesive as binder, serving as analogs to the three rock types (Fig. 2).

These samples were precisely weighed and then subjected to the same experimental conditions as the natural rocks. A total of 31 mixtures were employed to afford precise control over compositions, facilitating the evaluation of laser perforation in the various experiments. The samples underwent irradiation at 50 W for 180 s to faithfully replicate the mineral melting and evaporation processes observed in natural rocks. Temperature profiles were recorded throughout the experiments in combination with observations of the glazed layer and floccules, to explain the influence of rock composition on resulting temperatures from the perspective of mineral phase changes.

3. Impact of melt properties on thermal state

3.1. Characteristics of equilibrium thermal state

The equilibrium thermal state refers to the final stage in laser rock breaking when the melt volume remains constant and the temperature distribution remains constant in time. During this stage the energy consumption in transforming the rock phase gradually increases, leading to a decline in rock-breaking efficiency.

During laser irradiation, heat energy absorbed from the rock surface is conducted to the interior, generating a temperature gradient inside the rock. This gradient drives differential strains that result in thermal cracking and melting. The molten material further absorbs heat and undergoes evaporation. As the temperature rises, rock damage intensifies, with energy consumption primarily driven by the latent heat required for phase changes. The process of rock breaking can be viewed as an equilibrium (steady state) process at this stage. During this equilibrium stage, energy consumption mainly contributes to the generation of new molten material, while the elevated temperatures lead to rock softening, thus impeding the progression of thermal cracking [27]. High-speed digital imaging observations indicate a significant reduction in evaporation during this equilibrium stage (Fig. 3).

According to the distribution of measured temperatures, the rock sample exposed to a focused laser exhibits the development of three distinct regions, progressively distant from the focal point: an evaporation region, a melt region and heat diffusion region (Fig. 4). These three regions may be represented using a series of one-dimensional models with a uniform cross-sectional shape corresponding to the laser's point of contact.

Assuming that the rock is an equivalent isotropic continuum, we define the temperature distribution by considering energy balance, heat transport satisfying Fourier's law and energy consumed by phase change and liberated as latent heat. Thus, three typical heat-affected regions were divided. A surface evaporation region (V_t) contacts a melt region (V_m) and below this is a thermal diffusive region (V_t).

The basal heat diffusion region V_t is the region where only diffusive heat transfer occurs, absent melting and evaporation reactions. Temperatures throughout this region remain higher than the ambient tem-

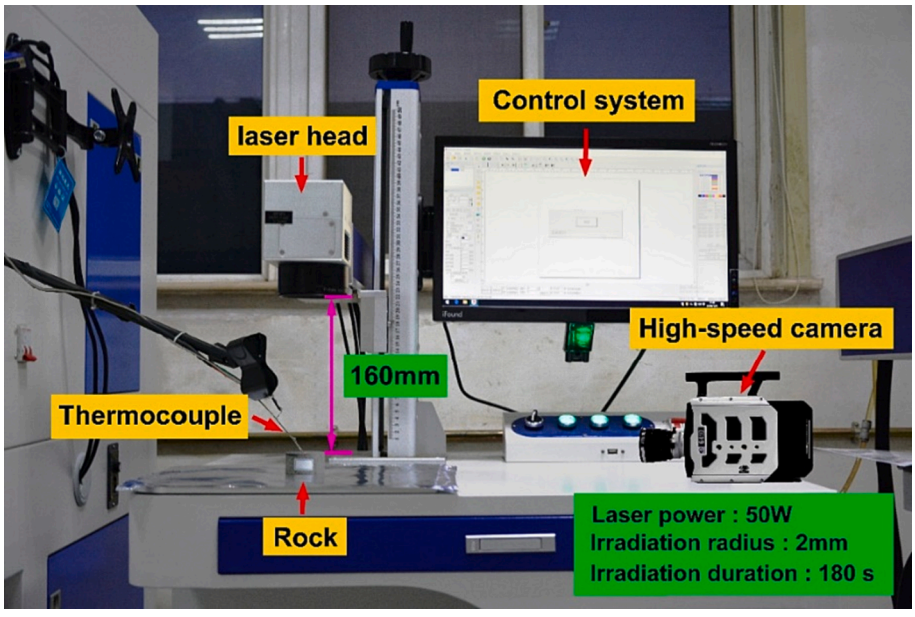

Fig. 1. Imaging and temperature measuring system for laser rock breakage.

Table 1
Mineral compositions of the rock samples.

Rock	Quartz	Pyroxene	Calcite	Feldspar	Hematite	Clay	Hornblende	Laumontite
Granite	49.5 %	–	1.6 %	29.2 %	–	19.7 %	–	–
Sandstone	37.0 %	–	2.3 %	48.9 %	3.3 %	7.6 %	–	0.9 %
Basalt	10.5 %	12.8 %	10.8 %	47.3 %	–	5.9 %	12.7 %	–

Table 2
Phase transition temperature of the three principal component minerals for the synthetic rock samples.

Rock component	Melting point (℃)	Evaporation temperature (℃)
Quartz	1715[a]	2230[a]
Feldspar	1290[a]	1540[a]
Kaolinite	1910[b]	–

[a] data from literature [25], [b]data from literature [26].

perature T_s and lower than the melting temperature T_m ($T_s \leq T \leq T_m$). Therefore, heat moving in and out is completely transformed into stored thermodynamic energy.

$$\frac{\partial T}{\partial t} = \frac{\lambda}{\rho c}\nabla^2 T \tag{1}$$

where T is temperature, t is time, λ is thermal conductivity, ρ is density, c is specific heat capacity and ∇^2 is the differential operator.

The melt region V_m is the region where melting has occurred, but where none of the minerals are yet evaporated. Temperatures within this region exceed the melting temperature but are insufficient to result in evaporation ($T \geq T_m$). In this region, thermal energy is absorbed both as sensible heat transport and as latent heat in melting and may be represented as (Eq. (2)):

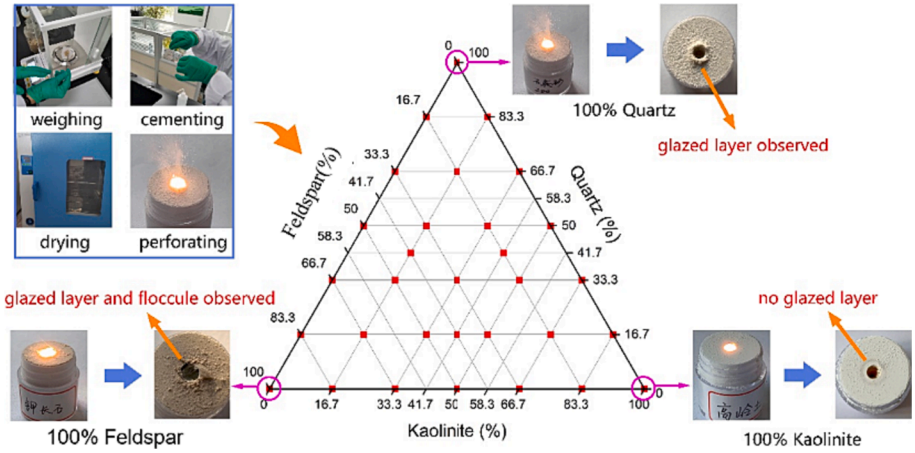

Fig. 2. Schematic of fabrication process and proportions of mineral components used in the synthetic rock samples.

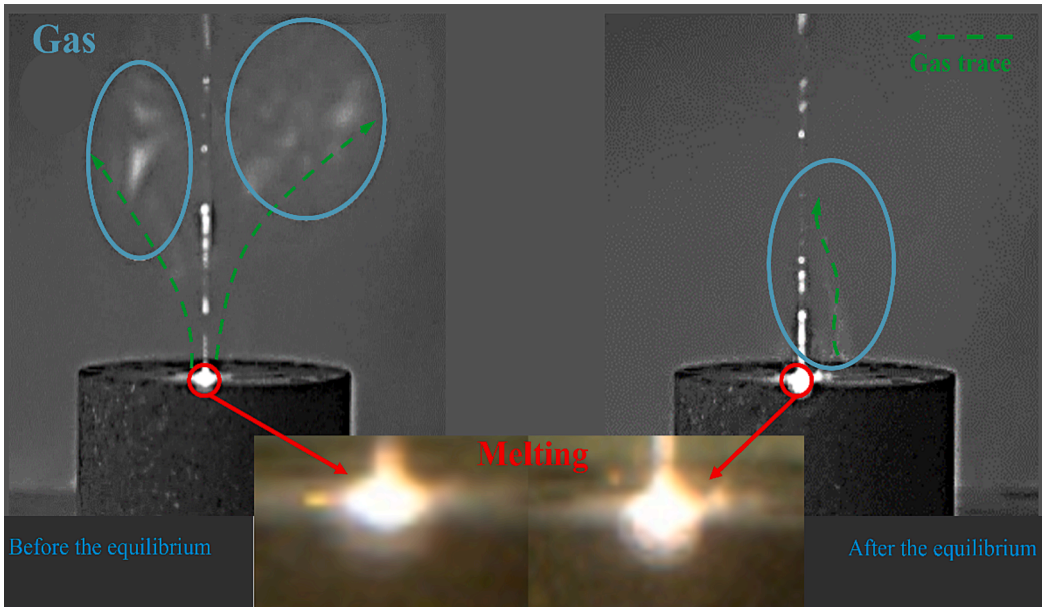

Fig. 3. Evaporation of the rock sample before and after reaching equilibrium captured by high-speed camera.

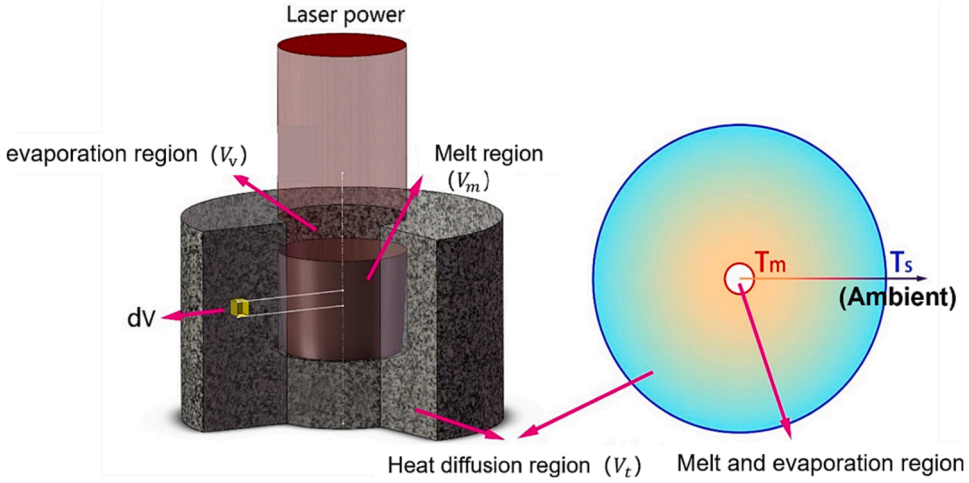

Fig. 4. The schematic of the melt and evaporation region of rock after laser irradiation.

$$\frac{\partial T}{\partial t} = \frac{\lambda}{\rho c}\nabla^2 T - L_1\frac{\partial f_1}{\partial t} \tag{2}$$

where f_1 is the liquid mole fraction, and L_1 is the latent heat of melting.

The evaporation region V_v is located above the melting region in direct contact with the surface that is impinged by the laser radiation. With the absorption of energy by the molten pool, evaporation occurs continuously. However, as irradiation time increases, the volume of the molten pool no longer changes, and the absorbed laser energy is dedicated solely to sustaining this slowly descending molten pool. No more evaporation occurs, so the volume of the evaporation region remains unchanged after entering the equilibrium stage, characterized by a constant rate of evaporation.

This quasi-equilibrium state represents a condition of steady-state heat transfer in which the melt volume remains constant and the temperature distribution in the heat diffusion region remains unchanged. A requirement is that the rate of melting zone advancement is significantly slower than the rate of heat transfer through conduction. Therefore, the melt volume and the temperature distribution in the heat diffusion region are critical parameters that describe this equilibrium stage. It is worth noting that both large melt volumes and excessively-high temperatures result in the wasteful consumption of laser energy and should be avoided.

3.2. Impact of melt properties on laser perforation

3.2.1. Melting volume per unit power

The expansion of the molten region will reach its limit when the surplus energy is entirely devoted to mineral evaporation. At this time, the volume of molten material will stabilize while descending slowly as minerals evaporate from the upper surface. During this phase, the expenditure of latent heat in the molten region becomes the predominant component of energy consumption.

Feldspar is a common component in rocks that is easy to melt by laser irradiation. The relationship between the melt volume of typical feldspars and laser power in this equilibrium state is shown in Fig. 5.

According to Fig. 5, at the equilibrium stage and low power levels, melt volume shows a proportional relationship with laser energy and may be defined as:

$$P_a = \alpha P = V_m q_{vm} + P_0 \tag{3}$$

where P_a is the laser energy absorbed by the rock surface, P_0 is a constant representing the heat loss due to convection and radiation, α is laser absorptivity, P is laser power and V_m is melt volume. q_{vm} is defined as melt volume per unit power, characterizing a melt property of the rock. According to Eq. (3), melt volume depends on q_{vm} of rock when laser power is fixed.

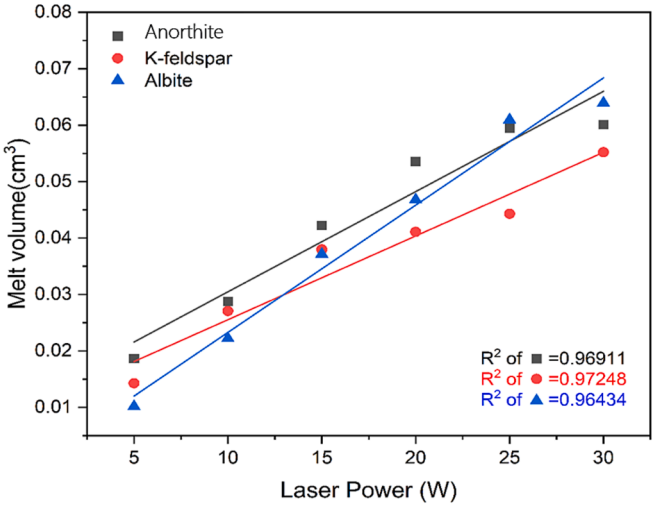

Fig. 5. Effect of laser power on melt volume.

3.2.2. Melting temperature

Temperature in the heat diffusion region remains constant when reaching the equilibrium state ($\frac{\partial T}{\partial t} = 0$). Assuming that the melt region is long compared to its diameter, then the principal 1D conduction of heat will be radially outwards from the melt region (Fig. 4). In cylindrical coordinates,

$$\frac{\partial^2 T}{\partial r^2} + \frac{1}{r}\frac{\partial T}{\partial r} + \frac{\partial^2 T}{\partial z^2} = 0 \tag{4}$$

and the boundary conditions for the heat diffusion region are

$$\begin{cases} T|_{r=r_1} = T_m \\ -\lambda\dfrac{\partial T}{\partial \boldsymbol{n}}\Big|_{r=r_2} = q_r + q_c \end{cases} \tag{5}$$

where T_m is melting temperature, r_1 is the radius at the contact surface with the melt, r_2 is the contact surface on the outer sample with the air, and n represents the normal vector of the contact surface.

Heat loss due to radiation q_r and convection q_c are

$$\begin{cases} q_r = \varepsilon_e \sigma_b \left(T_s^4 - T_r^4\right) \\ q_c = \alpha_c (T_s - T_r) \end{cases} \tag{6}$$

where ε_e is the equivalent emissivity of the rock surface and σ_b is the Boltzmann constant. α_c is a convective coefficient and T_s and T_r represent the rock surface temperature and the ambient air (room) temperature, respectively.

As a consequence of these relations and their interdependencies, the equilibrium temperature T_e is determined by the thermal conductivity, emissivity, convective coefficient and particularly the melting temperature of rock.

3.3. Influence of mineral composition on equilibrium temperature

3.3.1. Equilibrium temperatures of rocks and individual minerals

The equilibrium state during laser rock perforating is affected by the melting properties of the rock, which in turn are closely related to rock composition.

Laser perforation experiments are completed on intact samples of granite, sandstone and basalt as well as on pure samples of feldspar, quartz, and kaolinite. The evolution of temperature within the heat affected region is shown in Fig. 6.

The Basalt sample comprises 47.3 % feldspar (Table 1) and 10.5 % quartz, thus its equilibrium temperature is very close to the equilibrium temperature of feldspar. The equilibrium temperature of quartz is 1793℃ and for feldspar is 1540℃. Granite and sandstone are both quartz-feldspar aggregates with granite having a higher proportion of quartz than sandstone, hence the equilibrium temperatures of granite are closer to that of the melting temperature of quartz. Notably, across all these rock types, the equilibrium temperature exhibits a strong correlation with the relative proportions of quartz and feldspar.

3.3.2. Influence of quartz and feldspar proportion on equilibrium temperature

Temperature measurements recorded during laser irradiation experiments on the synthetic/analog rocks were completed to analyze the influence of quartz and feldspar proportion on equilibrium temperature (Fig. 7).

As shown in Fig. 7a, the equilibrium temperature of all samples is distributed between the bounding minimum melting temperature of feldspar (1290℃) and the maximum melting temperature of kaolinite (1910℃) (Table 2). When the kaolinite content is 100 %, the equilibrium temperature reaches the highest point of all artificial rock samples,

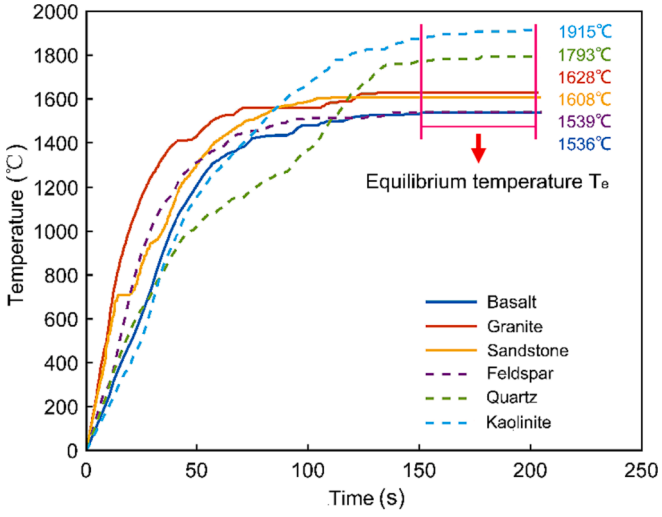

Fig. 6. Comparison of heat diffusion temperatures in rocks and individual minerals during laser perforating.

and no glazed layer is observed (Fig. 2). This suggests that the melting of kaolinite does not significantly influence equilibrium temperatures under this condition. Furthermore, the equilibrium temperature can be categorized into three distinct temperature ranges, delineated by the feldspar evaporation temperatureT_p = 1540℃ and the quartz melting temperatureT_g = 1750℃.

The influence of different component proportions on the range of equilibrium temperature is apparent in Fig. 7b. When the feldspar content is ≥ 16.7 % but quartz content is ≤ 33.3 %, then the equilibrium temperature will be close to or slightly lower than T_p, but cannot reach the melting temperature (T_g) of quartz. This indicates that the melt region is primarily influenced by the feldspar's melting, and the highest equilibrium temperature corresponds to the feldspar's evaporation temperature. When the content of feldspar is ≥ 16.7 % and the content of quartz is ≥ 33.3 % then the equilibrium temperature will be much higher than T_p and slightly lower than T_g. This indicates that the melt is dominated by the melting of quartz, but the presence of feldspar has a fluxing effect on that melting of quartz. When the feldspar content is ≤ 16.7 %, the equilibrium temperature is higher than T_g. This indicates that the feldspar content is too small to have a fluxing effect. Consequently, the quartz melt continues to absorb heat beyond its melting point until reaching equilibrium.

Therefore, equilibrium temperature is principally controlled by the melting of feldspar and quartz. The influence of feldspar and quartz content proportions on equilibrium temperature is shown in Fig. 8.

Fig. 8a shows that when the feldspar content is ≤ 16.7 %, the higher the content of feldspar, the lower the equilibrium temperature. Similarly, the higher the quartz content, the lower the equilibrium temperature.

Fig. 8b shows that when the feldspar content is ≥ 16.7 %, the equilibrium temperature will fluctuate within a narrow temperature range. The maximum temperature T_{max} is lower than the melting temperature of quartz T_g and the minimum temperature T_{min} is lower than the feldspar evaporation temperature T_p. This behavior primarily results from the fluxing effect of feldspar components on quartz. In addition, there is a defined proportion of quartz and feldspar where the equilibrium temperature is the lowest. Such component proportions in the rock reduce the energy loss caused by high temperatures in laser rock perforating and reduce the specific energy (SE) required for rock breaking.

4. Conclusions

A steady-state thermal conduction model of laser rock breaking is established based on an equilibrium melt model. In this model, the latent heat barrier controls both the melting and evaporation of component minerals and dominates the response. Conductive heat transfer plays a minimal role. The effect of rock composition on the laser-induced breaking mode is associated with the energy expended in the melting process. The relative equilibrium temperatures achieved through laser heating are evaluated through a set of laser perforation experiments. It is apparent from these that:

(1) A theoretical analysis shows that the melt volume within the melt region and the equilibrium temperature in the heat diffusion region are critical parameters to describe steady-state behavior during laser rock breaking. There is a linear relationship between melt volume and laser power, with the melt volume unit power controlled by rock compositions. The equilibrium temperature is determined by the thermal conductivity, emissivity, convective coefficient and the melting temperature of the rock.

(2) The equilibrium temperatures of sandstone, granite, and basalt, which depend on their mineral compositions, especially the amounts of feldspar and quartz, are different at laser irradiation. Equilibrium temperatures are divided into three temperature

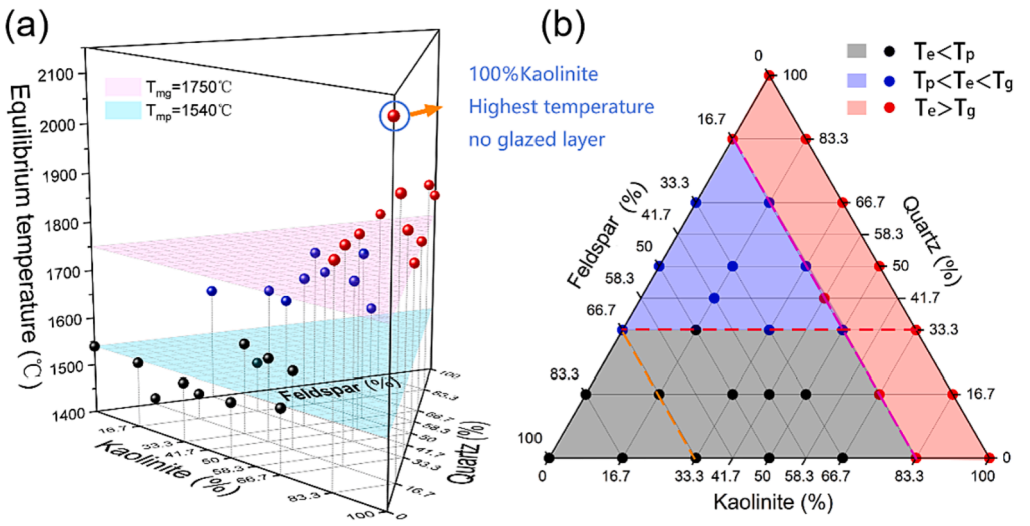

Fig. 7. Equilibrium temperatures for artificial rocks with different proportions of mineral components. (a) Equilibrium temperature ranges with composition; (b) classification by ternary diagram.

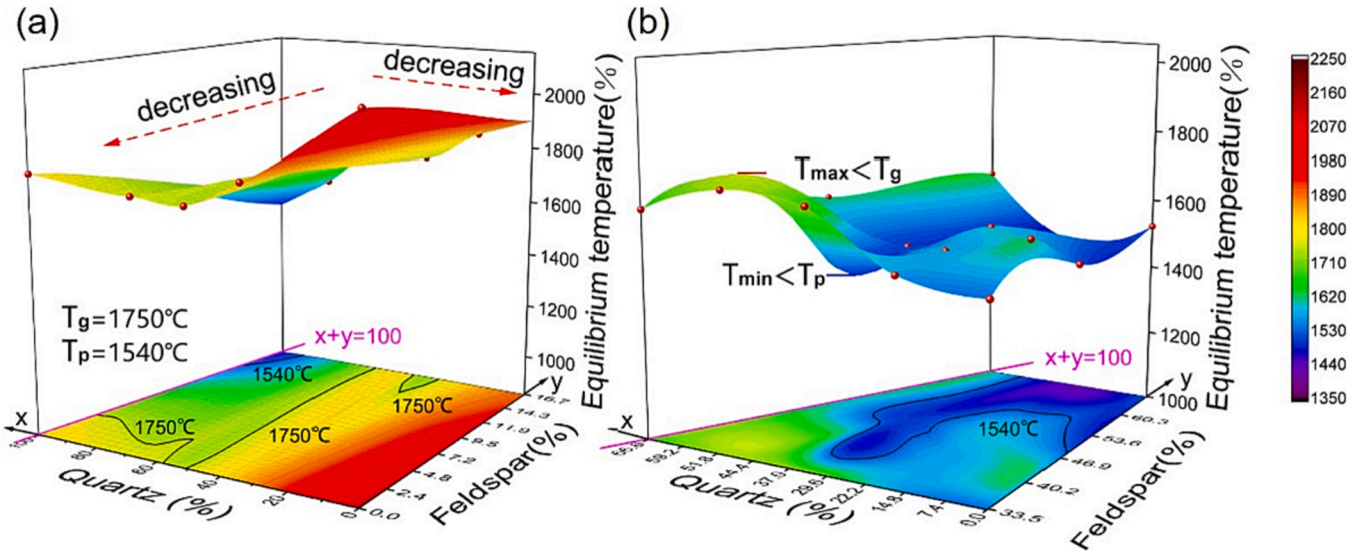

Fig. 8. Relationship between equilibrium temperature and the proportions of feldspar and quartz. (a) Feldspar content ≤ 16.7 %; (b) feldspar content ≥ 16.7 %.

ranges separated by the evaporation temperature of feldspar and the melting temperature of quartz. The first range is below the feldspar evaporation temperature, which occurs when the rock contains more than 16.7 % feldspar and less than 33.3 % quartz. The second range is between the feldspar evaporation temperature and the quartz melting temperature, which occurs when the rock contains more than 33.3 % quartz and any amount of feldspar. The third range is above the quartz melting temperature, which occurs when the rock contains less than 16.7 % feldspar and any amount of quartz.

Funding

This work is supported by the National Natural Science Foundation of China (Nos. U21B2072 and 51874310).

Declaration of competing interest

The authors declare that they have no known competing financial interests or personal relationships that could have appeared to influence the work reported in this paper.

Data availability

Data will be made available on request.

References

[1] D.G. O'Brien, R.M. Graves, E.A. O'Brien, StarWars Laser Technology for Gas Drilling and Completions in the 21st Century, SPE Annu. Tech. Conf. Exhib. (1999) 1–10.
[2] D. Bueso, M. Piles, G. Camps-Valls, Nonlinear PCA for Spatio-Temporal Analysis of Earth Observation Data, IEEE Trans. Geosci. Remote Sens. 58 (8) (2020) 5752–5763.
[3] F. Rui, G. Zhao, Experimental and numerical investigation of laser-induced rock damage and the implications for laser-assisted rock cutting, Int. J. Rock Mech. Min. Sci. 139 (2021), 104653.
[4] D. San-Román-Alerigi, C. van Dijk, V. Lube, G. Lubineau, Characterizing the Effects of High Power Laser Performance on Carbonate Rocks. In: 13th Middle East Geosciences Conference and Exhibition, 2018.
[5] Q.L. Yu, P.G. Ranjith, H.Y. Liu, T.H. Yang, S.B. Tang, C.A. Tang, S.Q. Yang, A Mesostructure-based Damage Model for Thermal Cracking Analysis and

Application in Granite at Elevated Temperatures, Rock Mech. Rock Eng. 48 (6) (2015) 2263–2282.
[6] C. David, B. Menéndez, M. Darot, Influence of stress-induced and thermal cracking on physical properties and microstructure of La Peyratte granite, Int. J. Rock Mech. Min. Sci. 36 (4) (1999) 433–448.
[7] Y. Jiao, X. Zhang, H. Zhang, H. Li, S. Yang, J. Li, A coupled thermo-mechanical discontinuum model for simulating rock cracking induced by temperature stresses, Comput. Geotech. 67 (2015) 142–149.
[8] T. Meier, D.A. May, P.R. von Rohr, Numerical investigation of thermal spallation drilling using an uncoupled quasi-static thermoelastic finite element formulation, J. Therm. Stresses. 39 (9) (2016) 1138–1151.
[9] R.A. Ndeda, S.E. Sebusang, R. Marumo, E.O. Ogur, Numerical model of laser spallation drilling of inhomogeneous rock, IFAC-PapersOnLine 50 (2) (2017) 43–46.
[10] B.M. Olaleye, A review of light amplification by stimulated emission of radiation in oil and gas well drilling, Min. Sci. Technol. 20 (5) (2010) 752–757.
[11] Z. Xu, Y. Yamashita, C. Reed, Modeling of Laser Spallation Drilling of Rocks for Gas and Oil Well Drilling, SPE Annu Tech Conf Exhib. (2005). SPE-95746-MS.
[12] O. Momin, S.Z. Shuja, B.S. Yilbas, CO2 laser heating of surfaces: Melt pool formation at surface, Opt. Laser. Technol. 44 (2) (2012) 463–470.
[13] H. Kariminezhad, H. Amani, M. Moosapoor, A laboratory study about laser perforation of concrete for application in oil and gas wells, J. Nat. Gas. Sci. Eng. 32 (2016) 566–573.
[14] S.Z. Shuja, B. Yilbas, O. Momin, Laser heating of a moving slab: Influence of laser intensity parameter and scanning speed on temperature field and melt size, Opt. Laser. Eng. 49 (2) (2011) 265–272.
[15] V. Sysoev, Y. Bulkin, High-dispersion amorphous quartz nanopowder received by CO2 laser radiation, SPIE Lasers Appl. Sci. Eng. 5713 (2005) 600–609.
[16] A. Adeniji, The Applications of Laser Technology in Downhole Operations - A Review, Int. Pet. Technol. Conf, IPTC, 2014.
[17] K. Nagai, M. Sato, H. Hattori, W. Sivakumaran, M. Kinugasa, Study on Rock Excavation with Laser, High-Power Lasers. Civ. Eng. Archit 3887 (2000) 57–66.
[18] R.M. Rauenzahn, J.W. Tester, Rock failure mechanisms of flame-jet thermal spallation drilling-theory and experimental testing, Int. J. Rock Mech. Min. Sci. Geomech. Abstr. 26 (1989) 381–399.
[19] S. Walsh, I. Lomov, J. Roberts, Geomechanical modeling for thermal spallation drilling, Geotherm. Resour. Counc. Trans. 35 (2011) 277–282.
[20] Z. Xu, C. Reed, R. Parker, B. Gahan, R. Graves, H. Figueroa, Laser rock drilling by a super-pulsed CO2 laser beam, Int. Congr. Appl. Lasers Electro-Optics. (2002), 160291.
[21] A. Bharatish, K.B. Kishore, R. Rajath, H.N. Narasimha Murthy, Investigation of effect of CO2 laser parameters on drilling characteristics of rocks encountered during mining, J. King. Saud. Univ-Eng Sci. 31 (4) (2019) 395–401.
[22] M. Hu, Y. Bai, H. Chen, B. Lu, J. Bai, Engineering characteristics of laser perforation with a high power fiber laser in oil and gas wells, Infrared Phys. Technol. 92 (2018) 103–108.
[23] X.Y. Yang, X. Zhou, H.L. Zhu, J.H. Zhou, Y.H. Li, Experimental Investigation on Hard Rock Breaking with Fiber Laser: Surface Failure Characteristics and Perforating Mechanism, Adv. Civ. Eng. (2020) 1–12.
[24] X.Y. Yang, J.H. Zhou, X. Zhou, A.G. Nie, Q. Jian, Investigation on the rock temperature in fiber laser perforating, Optik 219 (2020), 165104.
[25] W.A. Deer, R.A. Howie, J. Zussman, An introduction to the rock-forming minerals, Mineralogical Society of Great Britain and Ireland, London, 2013.
[26] J.W. Anthony, R.A. Bideaux, K.W. Bladh, M.C. Nichols, Handbook of Mineralogy, Tucson, Mineral Data Publishing, Arizona, 1997.
[27] F. Wang, H. Konietzky, Thermo-Mechanical Properties of Granite at Elevated Temperatures and Numerical Simulation of Thermal Cracking, Rock Mech. Rock Eng. 52 (10) (2019) 3737–3755.